HHS Public Access

Author manuscript

J Am Chem Soc. Author manuscript; available in PMC 2022 November 25.

Published in final edited form as:

J Am Chem Soc. 2021 June 23; 143(24): 9206–9214. doi:10.1021/jacs.1c04264.

Multiplex and In Vivo Optical Imaging of Discrete Luminescent Lanthanide Complexes Enabled by In Situ Cherenkov Radiation Mediated Energy Transfer

Kirsten E. Martin,

Alexia G. Cosby,

Eszter Boros

Department of Chemistry, Stony Brook University, Stony Brook, New York 11794, United States

Abstract

Recently, we pioneered the application of Cherenkov radiation (CR) of radionuclides for the in situ excitation of discrete Eu(III) and Tb(III) complexes. CR is produced by isotopes decaying under emission of charged particles in dielectric media and exhibits a maximum intensity below 400 nm. We have demonstrated that luminescent lanthanide antenna complexes are ideal acceptors for Cherenkov radiation-mediated energy transfer (CRET). Here, we develop and assess peptide-functionalized Tb(III) and Eu(III) complexes in conjunction with CRET excitation by the positron emissive radioisotope ^{18}F for simultaneous, multiplexed imaging and in vivo optical imaging. This work demonstrates, for the first time, that the detection of the luminescence emission of a discrete Eu(III) complex in vivo is feasible. Our results open possibilities for discrete luminescent lanthanide complexes to be used as diagnostic, optical tools for the intrasurgical guidance of tumor resection.

Graphical Abstract

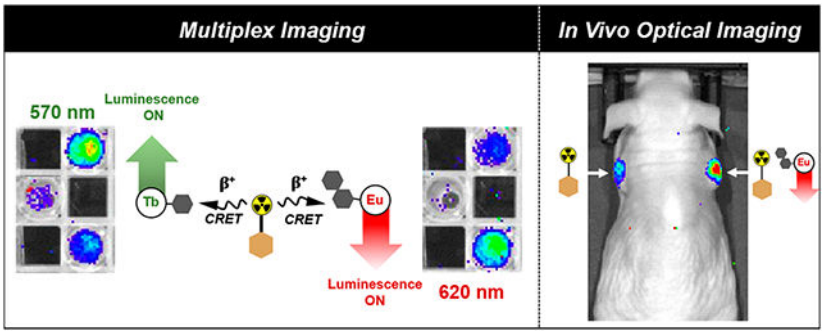

Corresponding Author Eszter Boros – Department of Chemistry, Stony Brook University, Stony Brook, New York 11794, United States; eszter.boros@stonybrook.edu.

Supporting Information

The Supporting Information is available free of charge at https://pubs.acs.org/doi/10.1021/jacs.1c04264.

Experimental procedures; NMR, HRMS, and HPLC results; characterization of complexes, and fluorescence imaging results (PDF)

The authors declare no competing financial interest.

INTRODUCTION

Lanthanide-based luminescence represents an attractive alternative to conventional organic chromophores used for biological imaging applications owing to (i) the unique electronic configuration of trivalent lanthanides which produces narrow emission bands independent of the metal coordinative environment, (ii) long luminescence lifetimes, and (iii) diminished photobleaching and self-quenching effects.[1,2] Emission maxima vary depending on the lanthanide, such as Tb(III), which emits green (λ_{em} = 490, 545 nm), or Eu(III), which emits red (λ_{em} = 613, 690 nm).[3]

Despite the advantages of lanthanide luminescence emission[4] and its increasingly widespread application in bioassays, lanthanide complexes have remained underexplored for bioimaging applications beyond cell assays and the imaging of translucent, multicellular organisms.[5,6] Due to the Laporte-forbidden nature of the 4f–f transitions, excitation of aromatic chromophores (“antennas”) followed by intersystem crossing and energy transfer is typically required to access lanthanide luminescence.[7,8] The antenna must possess a triplet state energy that is comparable to lanthanide acceptor states and thus allow efficient energy transfer with excitation wavelengths of 250–350 nm. This complicates bioimaging applications, as short-wavelength excitation light has very limited tissue depth penetration.

In order to circumvent the need for external excitation of luminescent lanthanide complexes, we have introduced the application of Cherenkov radiation (CR) as an in situ excitation source. Radioisotopes that meet the energy requirement to generate CR, such as positron emitters ^{18}F or ^{89}Zr,[9] provide an alternative source of short-wavelength light for lanthanide excitation.[10,11] CR in aqueous solutions is continuous, and its intensity exhibits a $1/\lambda^2$ dependence. As a consequence, intensity is significantly enhanced below 400 nm, which correlates well with the ideal excitation wavelengths of lanthanide antennas.[12-14] We have successfully established CRET as a means to excite discrete luminescent lanthanide complexes and employ CRET excitation to estimate quantum yields of Tb(III) complexes in a high-throughput manner.[15,16]

Motivated by our results, we posited that functionalized, high quantum yield Tb(III) and Eu(III) complexes bore potential for multiplexed and even targeted in vivo optical imaging when combined with a CR-emissive positron emission tomography (PET) radiopharmaceutical (Figure 1). The latter has been widely regarded as not feasible without specialized means of excitation such as two-photon excitation/upconversion and custom-built laser photon sources[6,17] and even if enabled, is further complicated by the need of exceedingly large quantities of lanthanide ion to produce a detectable luminescence signal. Indeed, the in situ excitation and in vivo imaging of luminescent quantum dots with CRET have been reported, but nanoparticles typically govern biological behavior and exhibit characteristic off-target uptake in the spleen, lungs, or liver.[18,19] Discrete molecular systems do not suffer from this predicament, yet have widely been considered not suitable to produce signal above the limit of detection even when compound quantities in the μmol range are employed.

Here, we demonstrate the feasibility of multiplexed imaging with discrete, luminescent Tb(III)- and Eu(III)-based imaging probes with optimized optical properties using conventional optical imaging equipment. We also probed the compatibility of these probes for in vivo imaging in conjunction with the widely clinically available PET tracer [^{18}F]-fluorodeoxyglucose (FDG) and show that targeted Eu(III) probes can produce a persistent emission signal in mouse tumor xenografts in vivo and ex vivo.

RESULTS AND DISCUSSION

Ligand Design and Complex Synthesis of Eu(III) Chelates.

Our first challenge represented the synthesis of an Eu(III) chelate with suitable optical and robust chemical properties to withstand implementation of bioconjugation. On the basis of our work on the CRET mediated excitation of Tb(III), complexes with quantum yields below 10% were not deemed suitable.[15,16] Competing, nonradiative de-excitation processes result in considerably lower quantum yields of Eu(III) complexes when compared with their Tb(III) analogues. While heteroarylalkyne linked antennas have been used extensively to produce inert, high quantum yield Eu(III) complexes suitable for time-resolved in vitro imaging,[20-24] the diminished solubility and incompatibility with acidic deprotection conditions commonly employed for orthogonal peptide conjugation chemistry were not desirable for our particular applications. Efficient energy transfer from the antenna T_1 to the $^5D_1$ Eu(III) excited state requires a T_1 energy of >22 000 cm^{-1} to enable efficient energy transfer to $^5D_1$ at 19 000 cm^{-1}.[25] Following the work of Quici et al, we synthesized a tetraazamacrocyclic-based chelator containing a phenanthroline antenna (DO3Aphen, Figure 2), which had been identified to produce robust Φ_{Ln} of >20%.[26]

Chemical synthesis was achieved following previously published procedures.[26,28] In short, commercially available dimethylphenanthroline was used to synthesize acetoxymethyl-phenathroline in two steps, which was deacetylated under basic conditions and mesylated for subsequent alkylation to DO3A-*t*Bu[29] (Scheme S1). Removal of the *tert*-butyl protecting groups under acidic conditions yields DO3Aphen, which was complexed with a europium triflate salt in water, by increasing the pH to between 7 and 7.5 with 0.1 M NaOH. Complex formation was monitored by analytical HPLC and observation of the characteristic europium-based red emission of the resulting complex [Eu(DO3Aphen)]. To probe the sensitivity of europium complexes to O—H mediated de-excitation, a monohydrated complex analogue $[Eu(DO2Aphen)]^+$ was also synthesized in analogous manner to [Eu(DO3Aphen)] using the protected macrocycle DO2A-*t*Bu[30] for alkylation, which was then deprotected under acidic conditions and complexed as described above (Scheme S2). We determined inner-sphere hydration number (q) of both complexes using Horrocks' equations and employed the established gradient-based method to determine quantum yield.[27,31,32] [Eu(DO3Aphen)] was confirmed to be a $q = 0$ complex and possesses a moderate quantum yield of 15%. The $[Eu(DO2Aphen)]^+$ complex was confirmed to be a $q = 1$ complex and, correspondingly, possesses a decreased quantum yield of 5%. This significant decrease in quantum yield highlights the necessity for europium complexes to efficiently exclude inner-sphere hydration for viable applications in the context of CRET imaging (Table 1).

The kinetic inertness of [Eu(DO3Aphen)] and [Tb(DO3Apic)]$^{-}$ was investigated with a diethylenetriaminepentaacetic acid (DTPA) challenge.[33-35] In presence of 1000× excess DTPA in Dulbecco's phosphate buffered saline (DPBS, pH 7.4), the antenna absorption peak of [Eu(DO3Aphen)] remained centered at 285 nm (characteristic of complex) rather than 275 nm (characteristic of unchelated ligand), indicating no transchelation occurred over 14 days. Additionally, the retention time of the samples remained consistent with that of the complex (t_R complex, 5.02 min; t_R ligand, 4.85 min), further affirming that the DO3Aphen scaffold was sufficiently inert for prospective biological applications (Figures S53-S55). [Tb(DO3Apic)]$^{-}$ exhibited comparable kinetic stability under identical conditions (Figures S56-S58). Identical results were produced at pH 6.5, indicating that the complexes were sufficiently inert under conditions mimicking acidic tumor microenvironments (Figures S59 and S60).

Optical Imaging of Eu(III) Complexes Using CRET Excitation.

To assess the suitability of newly synthesized Eu(III) complexes and determine appropriate functionalization strategies, we evaluated the CRET-mediated excitation of the nonfunctionalized model complexes using optical imaging of phantoms containing 10 μCi of Na^{18}F. We selected this quantity of radioactivity as this is a typical quantity of activity used in in vivo PET imaging.[36,37]

Solutions of 1–150 nmol of [Eu(DO3Aphen)] and [Eu(DO2Aphen)]$^{+}$ in DPBS were doped with 8 μCi of Na^{18}F and imaged on a conventional small animal scanner, with blocked excitation and emission collected from 500 to 845 nm (Figure 3). Region of interest (ROI) analysis revealed increased signal intensity of [Eu(DO3Aphen)] compared to [Eu(DO2Aphen)]$^{+}$, a result in accordance with their respective quantum yields: significant decrease in radiance was observed for the [Eu(DO2Aphen)]$^{+}$ complex (Figure S63). Radiance of [Eu(DO3Aphen)] could be detected with a limit of detection (LOD) of 10 nmol of complex, while [Eu(DO2Aphen)]$^{+}$ possessed a significantly increased limit of detection of 50 nmol underscoring that quantum yields of at least 10% are required for the detection of biologically relevant optical probe compound concentrations.

Multiplex Optical Imaging.

The differential optical emission properties of the Eu(III) and Tb(III) complexes enable detection at different wavelengths of emission (Figure 4A). To validate this concept, we carried out CRET imaging experiments with the nonfunctionalized Eu(III) and Tb(III) complexes. The previously studied [Tb(DO3Apic)]$^{-}$ complex was synthesized as described[15] and solutions of 0.4–80 nmol of [Eu(DO3Aphen)] and [Tb(DO3Apic)]$^{-}$ in DPBS were doped with 10 μCi of Na^{18}F and imaged (Figure 4C). Emission of the two complexes was observed using 40 nm bandpass emission filters centered at 570 and 620 nm. Region of interest (ROI) analysis (Figure 4B) revealed that for complex quantities of 10 nmol with imaging centered at 570 nm, emission of [Tb(DO3Apic)]$^{-}$ was 4.6× greater than that of [Eu(DO3Aphen)]. At the same concentration with wavelength detection centered at 620 nm, emission of [Eu(DO3Aphen)] was 5.3× greater than that of [Tb(DO3Apic)]$^{-}$. Discernable, wavelength selective emission was detected with probe as little as 4 nmol. This initial proof-of-concept study validates the feasibility of multiplexed optical imaging

using Eu(III) and Tb(III) complexes and can enable the simultaneous imaging of two targets without the need for time-resolved spectral deconvolution.[5,38]

Synthesis of Targeted Peptide Conjugates.

To assess the use of discrete Tb(III) and Eu(III) complexes for targeted applications, conjugated versions of model complexes were synthesized. The phenanthroline-based system was functionalized using the linker-functionalized dipeptide, 2-[3-(1,3-dicarboxypropyl)ureido]pentanedioic acid (DUPA). DUPA targets the prostate-specific membrane antigen (PSMA),[39] which is highly overexpressed in metastasizing prostate cancer cells[40] and serves as an ideal initial proof-of-concept targeting vector. A variety of PSMA targeting fluorophores have been studied in preclinical animal models.[41-43] The functionalized ligand, (DO2Aphen)-DUPA), was synthesized stepwise from the *tert*-butyl protected DO2Aphen ligand (Scheme S3). A benzylbromoacetate arm was installed under stepwise alkylation conditions; however, the subsequent debenzylation of the orthogonally protected carboxylic acid proved difficult, as under even mild conditions, significant concomitant loss of the phenanthroline antenna occurred. Mixtures of unreacted starting material, the expected product, and material lacking the antenna while still retaining the benzyl arm were produced. Though these products could be easily separated by HPLC purification, the overall yield of desired product was significantly reduced. The orthogonally protected ligand was then amidated with the *tert*-butyl protected form of aminopentyl-functionalized DUPA (Scheme S3).[34] The ligand was deprotected and complexed as described above to afford a functionalized molecule, $[Eu(DO2Aphen)\text{-}DUPA]^{+}$. The corresponding complex was characterized for its photophysical properties and exhibited a slight decrease in quantum yield, (Φ_{Ln} = 10%, Table 1) despite confirmation of a $q = 0$ complex. Likely through steric bulk or direct coordination of the amide, the coordination environment excludes the coordination of a water molecule.

As a corresponding Tb(III)-based probe, we capitalized on established chemical synthesis and characterization to produce [Tb(DO2Apic)-DUPA]. The corresponding functionalized version of the ligand had been successfully synthesized and characterized in the context of imaging with lanthanum isotopes.[34] We pursued the previously reported synthetic approach to produce the corresponding Tb(III) complex, which produced a quantum yield Φ_{Tb} = 38% and retained the ability to exclude inner sphere hydration in accordance with the nonfunctionalized parent Tb(III) complex.

Following synthesis and photophysical characterization (Table 1), we conducted a multiplex imaging experiment in direct analogy with the nonfunctionalized compounds and found that discernible wavelength-selective luminescence emission using 570 or 620 nm bandpass filters was retained (Figure S65).

In Vitro and in Vivo Optical Imaging for Targeted Complexes.

With PSMA-targeting constructs in hand, we sought to investigate the potential of these compounds to be utilized as optical probes in vivo. We posited that [^{18}F]-FDG, a PET imaging agent targeting GLUT-1, overexpressed in most cancer subtypes, may be ideally suited to serve as an in situ CRET source (Figure 1). First, we determined the ability

of [Tb(DO2Apic)-DUPA] and [Eu(DO2Aphen)-DUPA]$^+$ to produce luminescence emission that exhibits tissue penetration. Figure 5A and Figure 5B show phantoms imaged before (A) and after (B) the introduction of a 2 mm muscle tissue slice. Compound quantities were selected in accordance with the previously determined LODs, and 20 μCi of Na^{18}F was employed as a CRET only reference and as an in situ excitation source for all samples. As visible in Figure 5B, both [Eu(DO2Aphen)-DUPA]$^+$ samples (10 and 40 nmol) provide detectable emission, while the CRET only and Tb(III)-mediated signal is efficiently attenuated by tissue. The emission of the Tb(III) complex is predominantly green (λ_{em} = 490, 545 nm) and thus attenuated more strongly. Additionally, we hypothesize that the comparably low Φ_{Ln} quantum yield of <40% may also contribute to failure to detect the corresponding emission.

Efficient tissue penetration of red-emissive Eu complexes motivated evaluation of CRET-mediated excitation of the targeted [Eu(DO2Aphen)-DUPA]$^+$ in a murine xenograft PSMA-expressing tumor model. To closely control administered activity and optical probe, we chose intratumoral administration of either only 22 μCi [^{18}F]-FDG or 40 nmol of [Eu(DO2Aphen)-DUPA]$^+$ coadministered with 22 μCi [^{18}F]-FDG. Mice were subsequently imaged at 8 min postinjection (Figure 5C), followed by tumor resection and ex vivo imaging of the two masses at 1 and 3 h postinjection (Figure 5D). Both in vivo and ex vivo images demonstrate detectable luminescence emission by the [Eu(DO2Aphen)-DUPA]$^+$ construct, even after prolonged exposure, partial radioactive decay, and clearance of the Eu(III) probe. Inductively coupled plasma optical emission spectroscopy (ICP-OES) revealed that the tumor had retained 0.78 nmol of Eu(III) probe, yet ex vivo imaging in the presence of 27 μCi and 13 μCi of [^{18}F]-FDG provided excellent tumor conspicuity, indicating that prospective, systemic administration of detectable Eu(III) probe doses is feasible. We currently cautiously hypothesize that an increased blue light emission of tissue (n > 1.35) with a refractive index greater than water (n = 1.33) is responsible for the detectability of the Eu(III) emission in vivo. Experiments to investigate this effect are ongoing.

CONCLUSIONS

The magnetic and optical properties of discrete lanthanide complexes provide unique opportunities for bioimaging applications. Undoubtedly, Gd(III)- or Eu(II)-based magnetic resonance imaging (MRI) has long been considered the most compatible with targeted in vivo imaging using discrete molecular complexes. In vivo optical imaging, while conceptually feasible as lanthanides Eu(III), Sm(III), Tm(III), Ho(III), Yb(III), and Nd(III) emit in the NIR optical window, has remained underexplored due to inherently low Φ_{Ln} and/or indirect means of excitation which require tissue-impermeable, short wavelength excitation.

Here, we show for the first time that in situ excitation of discrete Tb(III) and Eu(III) complexes using Na^{18}F as a CRET source enables multiplex imaging using conventional optical imaging equipment. Optical imaging of Tb(III) or Eu(III) phantoms in the presence of a CRET source is possible at concentrations as low as 4 nmol (20 μM) and in vivo optical imaging as low as 10 nmol (50 μM) with Eu(III). Of note, this represents an order of magnitude lower probe concentration as what is typically required for Gd(III)-enhanced

MRI imaging[44-46] or for organic sensor probes.[47-50] The required probe concentration can be further lowered by enhancing the quantum yield Φ_{Ln}, especially for Eu(III) probes, further decreasing the limit of detection by at least 1 order of magnitude, in line with targeted, organic optical probes.[51-53] Efforts to enhance Φ_{Eu} of conjugated Eu(III) complexes while retaining aqueous solubility and devising means to systemically administer both the CRET source and lanthanide probe to illuminate cancer targets in an orthotopic tumor model are currently ongoing.

Lastly, we highlight that our work unlocks targeted, luminescent lanthanide coordination complexes as a to-date untapped compound class with potential for in vivo optical imaging.

EXPERIMENTAL SECTION

All starting materials were purchased from Acros Organics, Alfa Aesar, Macrocyclics, Sigma-Aldrich, or TCI America and used without further purification. NMR spectra (^{1}H, ^{13}C) were collected on a 700 MHz Advance III Bruker, 500 MHz, or 400 MHz Bruker instrument at 25 °C and processed using TopSpin 4.0.7. Chemical shifts are reported as parts per million (ppm). Low-resolution electrospray ionization (ESI) mass spectrometry and high-resolution (ESI) mass spectrometry were carried out at the Stony Brook University Center for Advanced Study of Drug Action (CASDA) with a Bruker Impact II UHR QTOF MS system. UV–vis spectra were collected with the NanoDrop ^{1}C instrument (AZY1706045). Spectra were recorded from 190 to 850 nm in a quartz cuvette with 1 cm path length. Luminescence measurements were carried out on a Hitachi F-7100 FL spectrophotometer. Wavelength scans were collected by exciting at the appropriate wavelength (283 nm for Eu(III) and 282 for Tb(III)) for antenna-mediated excitation and minimization of scattering interference. Emission spectra were collected from 300 to 800 nm, with 1.0 nm excitation and 5.0 nm emission slit widths, 1200 s scan time, 0.05 s response time, and PMT voltage = 400 V. Quantum yield measurements for europium were carried out using $Ru(bipy)_3$ as standard (λ_{ex} = 450 nm). Terbium quantum yield measurements used $[Tb(DO3Apic)]^{-}$ (QY= 47%) as a standard. Lifetime measurements were executed using the following settings: scan time 20 ms; chopping speed of 40 Hz; excitation wavelength of 255.0 nm (with the exception of $[Eu(DO2Aphen)]^{+}$ which was excited at 285.0 nm) and emission wavelength of 555.0 nm; 0 s delay; excitation and emission slit widths of 10 nm each; 0.5 s response. Complexes were dissolved in H_2O or D_2O, and samples were resuspended and lyophilized in D_2O repeatedly prior to measurement. A quartz cuvette with a 1 cm path length was used. ICP-OES was carried out using an Agilent 5110 inductively coupled plasma optical emission spectrometer. A 10-point standard curve or a 6-point standard curve with a check standard with respect to europium or terbium was used, and fits were found to be at least R^2 of 0.999. Concentrations were then back calculated to the stock sample concentration. IVIS Lumina series III from Caliper LifeSciences small animal imager was used for imaging. All scans were collected with blocked excitation and either open emission filter or selected emission filters as discussed. The open emission filter runs from 500 to 875 nm, with an average bandwidth of 20 nm and a collection time of 5 min. Images were analyzed with Living Image software (version 4.3.1). Preparative HPLC was carried out using a Shimadzu HPLC-20AR equipped with a binary gradient, pump, UV–vis detector, manual injector on a Phenomenex Luna C18

column (250 mm × 21.2 mm, 100 Å, AXIA packed). Method A (preparative purification method): A = 0.1% TFA in water, B = 0.1% TFA in MeCN. Gradient, 0–5 min: 95% A. 5–24 min: 5–95% B gradient. Analytical reversed phase HPLC of compounds was performed with a Shimadzu system, equipped with a CBM-20A interface, SIL-20A HT autosampler, SPD-20AV UV detector, LabLogic dual scan-RAM radio-HPLC detector, and a LC-20AB pump. A reversed-phase C18 column (Phenomenex Luna 5 μm C_{18}(2) 100 Å, LC column 150 mm × 3 mm) was used for analytical purposes. The mobile phase consisted of 0.1% TFA in deionized water (A) and 0.1% TFA acetonitrile (B). A gradient of solvent B (5–95% over 20 min) at a flow rate of 0.8 mL/min was used for analytical characterization runs (method C).

Synthesis of [Eu(DO2Aphen)-DUPA]$^+$.

Benzyl{7-[(6-methyl-4,5-diaza-3-phenanthryl)methyl]-4,10-bis(tert-butoxycarbonylmethyl)-1,4,7,10-tetraaza-1-cyclododecyl}acetate (7).—Benzyl bromoacetate (2.9 μL, 0.018 mmol), 6 (7.4 mg, 0.012 mmol), and K_2CO_3 (16.9 mg, 0.122 mmol) were combined in dry MeCN (5 mL) and refluxed overnight. K_2CO_3 was filtered out, and the filtrate was concentrated. The resulting residue was purified using reverse phase preparative HPLC (method A) with pure product eluting at 16.6 min. Fractions containing product were pooled and solvent was removed in vacuo to afford pure 7 (4.7 mg, 51% yield). ^{1}H NMR (CD_3OD, 700 MHz): δ 9.06 (br s, 1H), 8.24 (m, 5H), 7.44 (m, 5H), 5.36 (s, 2H), 5.19, 4.16 (s, 2H), 4.03–3.33 (m, 16H), 3.30–3.02 (m, 16H), 3.19 (s, 3H), 1.40 (s, 18H). ^{13}C{^{1}H} NMR (CD_3OD, 175 MHz): δ 174.2, 167.5, 159.5, 139.5, 137.3, 136.4, 130.7, 129.9, 129.6, 129.5, 129.3, 127.9, 127.9, 86.7, 84.0, 69.1, 67.5, 61.1, 60.1, 55.6, 49.8, 28.4, 21.6. ESI- MS calcd for $C_{43}H_{58}N_6O_6$: 754.44. Found: 755.4 $[M + H]^+$ and 378.3 $[M + 2H]^{2+}$.

{7-[(6-Methyl-4,5-diaza-3-phenanthryl)methyl]-4,10-bis(tert-butoxycarbonylmethyl)-1,4,7,10-tetraaza-1-cyclododecyl}acetic Acid (8).—To a solution of 7 (16.6 mg, 0.022 mmol) in MeOH (5 mL), a suspension of Pd/C (1.2 mg, 7% w/w) in MeOH (1 mL) was added. The flask was evacuated and charged with H_2 (1 atm), and then the mixture was stirred at room temperature for 5 h. The reaction mixture was filtered, and the solvent was removed in vacuo. The resulting oil was purified with reverse phase preparative HPLC (method A) with the product eluting at 13.6 min. The fractions containing product were combined and the solvent was removed in vacuo to afford **8** (5.4 mg, 37% yield). ^{1}H NMR (CD_3OD, 700 MHz): δ 8.63 (s, 1H), 8.57 (d, 1H), 8.09 (d, 1H), 8.05 (d, 1H), 8.00 (s, 1H), 7.89 (d, 1H), 4.93 (s, 2H), 3.96–3.44 (m, 12H), 3.29–3.03 (m, 8H), 3.02 (s, 3H), 1.20 (s, 18H). ^{13}C{^{1}H} NMR (175 MHz, CD_3OD): δ 172.3, 160.5, 139.3, 130.5, 129.5, 129.2, 128.4, 127.6, 126.6, 126.5, 83.5, 59.4, 55.5, 55.3, 52.7, 50.4, 49.5, 28.3, 24.2. ESI-MS calcd for $C_{36}H_{52}N_6O_6$: 664.39. Found: 665.4 $[M + H]^+$ and 333.4 $[M + 2H]^{2+}$.

Di-tert-butyl 2-(3-{4-[5-(2-{7-[(6-methyl-4,5-diaza-3-phenanthryl)methyl]-4,10-bis(tert-butoxycarbonylmethyl)-1,4,7,10-tetraaza-1-cyclododecyl}acetylamino)pentylamino]-4-oxo-1-tert-butoxycarbonylbutyl}ureido)glutarate (9).—8 (1.5 mg, 0.002 mmol) was

added to a solution of DIPEA (0.45 λL, 0.027 mmol) and HBTU (1.3 mg, 0.003 mmol) in DMF (5 mL). The mixture was allowed to stir for 15 min, and then a solution of *di-tert*-butyl (*R*)-2-(3-((*R*)-4-(5-aminopentylamino)-4-oxo-1-*tert*-butoxycarbonylbutyl)ureido)glutarate[34] (1.3 mg, 0.002 mmol) in DMF (2 mL) was added. The reaction was stirred overnight at room temperature, and the solvent was then removed in vacuo. The crude product was purified using reverse phase preparative HPLC (method A) with the product eluting at 19.2 min (1.6 mg, 58% yield). ^{1}H NMR (CD_3OD, 700 MHz): δ 8.71 (s, 1H), 8.61 (s, 1H), 8.24 (s, 1H), 8.12 (q, 2H), 7.95 (s, 1H), 5.02 (s, 2H), 4.22 (m, 1H), 4.15 (m, 1H), 3.98 (s, 2H), 3.93–2.91 (m, 20H), 3.67 (s, 4H), 3.19 (m, 4H), 3.06 (s, 3H), 2.28 (m, 4H),2.08 (m, 2H), 1.84 (m, 2H), 1.50 (m, 4H), 1.49, 1.47, 1.32 (s, 45H), 1.38 (m, 2H). ESI-MS calcd for $C_{64}H_{102}N_{10}O_{13}$: 1218.76. Found: 1219.8 $[M + H]^+$ and 610.6 $[M + 2H^+]^{2+}$.

2-(3-{4-[5-(2-{4,10-Bis(carboxymethyl)-7-[(6-methyl-4,5-diaza-3-phenanthryl)methyl]-1,4,7,10-tetraaza-1-cyclododecyl}acetylamino)-pentylamino]-1-carboxy-4-oxobutyl}ureido)glutaric Acid ((DO2Aphen)-DUPA).—9 (1.6 mg, 0.001 mmol) was dissolved in a solution of 1:2 DCM/TFA (1.5 mL) and stirred at room temperature overnight. The solvent was removed in vacuo, and the product was redissolved in H_2O. The solution was then lyophilized to yield (DO2Aphen)-DUPA as a white solid (0.8 mg, 65% yield). ^{1}H NMR (CD_3OD, 700 MHz): δ 8.98 (d, 1H), 8.70 (s, 1H), 8.22 (q, 2H), 8.12 (d, 2H), 4.97 (s, 2H), 4.27 (q, 1H), 4.23 (q, 1H), 4.02 (br s, 2h), 3.66–3.05 (m, 16h), 3.51 (m, 4H) 3.16 (s, 3H), 2.38 (m, 2H), 2.31 (m, 2H), 2.16 (m, 2H), 2.11 (m, 2H), 1.86 (m, 4H), 1.59 (m, 4H), 1.42 (m, 2H). HRMS calcd for $C_{44}H_{62}N_{10}O_{13}$: 938.4498. Found: 939.4560. HPLC: t_R = 6.3 min (method C).

Synthesis and Characterization of Eu Complexes.

To a solution of ligand dissolved in water, 1 equiv of $Eu(OTf)_3$ salt was added. The pH was adjusted to 7.0–7.5 using 0.1 M NaOH. The complex was then purified via SepPak (Waters Sep-Pak C_{18} Plus short cartridge, 360 mg sorbent per cartridge, 55–105 μm particle size). The fractions containing product were pooled and lyophilized, yielding white solids. [Eu(DO3Aphen)] product eluted in 90:10 (H_2O/MeCN). HRMS calcd for $C_{28}H_{33}EuN_6O_6$: 702.1674, 700.1660. Found: 723.1546 $[M + Na]^+$. R_t = 5.7 min (method C). $[Eu(DO2Aphen)]^+$ product eluted in 90:10 (H_2O/MeCN). HRMS calcd for $C_{26}H_{31}EuN_6O_4$: 644.1619. Found: 643.1675 and 645.1692 $[M + H]^+$. R_t = 5.7 min (method C). $[Eu(DO2Aphen)\text{-}DUPA]^+$ product eluted in 90:10 (H_2O/MeCN). HRMS calcd for $C_{44}H_{59}EuN_{10}O_{13}$: 1089.3554. Found: 1087.3538 and 1089.3558 $[M + H]^+$. R_t = 6.3 min (method C). The kinetic inertness of [Eu(DO3Aphen)] and $[Tb(DO3Apic)]^-$ was investigated with a diethylenetriaminepentaacetic acid (DTPA) challenge. The complexes in 1× DPBS (pH 7.4) [(Eu(DO3Aphen)], 1.85 mM, 20 μL; $[Tb(DO3Apic)]^-$, 0.48 mM, 230 μL) were combined with 1000× excess DTPA ([Eu(DO3Aphen)], 75 mM, 492 μL; $[Tb(DO3Apic)]^-$, 150 mM, 741 μL) and excess buffer (total volume of each sample, 2 mL), and the UV–vis spectrum and analytical HPLC trace were recorded over 14 days. UV–vis spectra were collected with the NanoDrop ^{1}C instrument (AZY1706045), and spectra were recorded from 190 to 850 nm in a quartz cuvette with 1 cm path length. For [Eu(DO3Aphen)] absorbance maximum at 285 nm is characteristic for the complex and at 275 nm it is characteristic of the unchelated ligand. The retention times of the complex and

uncomplex ligands were 5.02 and 4.85 min, respectively. For [Tb(DO3Apic)] absorbance maximum at 275 nm is characteristic for the complex and at 268 nm it is characteristic of the unchelated ligand. The retention times of the complex and uncomplex ligands were 1.55 and 1.52 min, respectively. UV–vis measurements were collected daily, and HPLC analysis was conducted every 48 h with a standard of complex and free ligand run alongside the challenge samples.

Phantom Preparation, Imaging, and Image Processing.

Concentrations of each lanthanide complex were diluted, and 200 μL aliquots of dilutions were prepared in 1× DPBS buffer to which 10 μL of $Na^{18}F$ (10 or 20 μCi) was added to produce a final volume of 210 μL. IVIS Lumina series III from Caliper LifeSciences small animal imager was used for imaging. All scans were collected with blocked excitation and either open emission filter or selected emission filters as discussed. The open emission filter measures from 500 to 875 nm, with an average bandwidth of 20 nm and a collection time of 5 min. Images were analyzed with Living Image software (version 4.3.1). Regions of interest (ROI) were determined in triplicate with the ROI tool for each concentration. Radiance values for each complex are subtracted from the Cherenkov-only sample ($Na^{18}F$ in 1× DPBS buffer).

In Vitro and in Vivo Imaging.

To assess the quenching effects of tissue, phantom images of $[Eu(DO2Aphen)\text{-}DUPA]^+$ and [Tb(DO2Apic)-DUPA] were collected in the presence of 2 mm turkey slices. Solutions of 10 and 40 nmol of $[Eu(DO2Aphen)\text{-}DUPA]^+$ and [Tb(DO2Apic)-DUPA] in 1× DPBS were doped with 20 μCi of $Na^{18}F$ and imaged. Turkey slices (2 mm thickness) were layered on top of the phantoms, and the samples were reimaged. All animal experiments and procedures were performed in accordance with the National Institutes of Health's "Guide for the Care and Use of Laboratory Animals" and approved by Institutional Animal Care and Use Committee (IACUC) at Stony Brook Medicine. Male Ncr mice (Taconic Biosciences, Rensselaer, NY) were inoculated subcutaneously on the right and left shoulders with 1.0×10^6 PSMA positive PC-3 PIP cells suspended in Matrigel (1:2 DPBS/Matrigel). When the tumors reached a suitable size, mice were anesthetized with isoflurane and a mixture of $[Eu(DO2Aphen)\text{-}DUPA]^+$ (40 nmol) and $[^{18}F]$-FDG (100 or 22 μCi, NCM-USA, Bronx, NY) was injected intratumorally to the right shoulder. A corresponding volume and activity of saline and $[^{18}F]$-FDG (100 or 22 μCi) were injected intratumorally to the left shoulder. Mice were imaged at 5 min (100 μCi) and 8 min (22 μCi) p.i. with the IVIS Lumina series III small animal imager. Mice were sacrificed 3 h p.i. (100 μCi dose) and 1 h p.i. (22 μCi dose), and tumors were extracted and imaged. Tumors were digested with concentrated nitric acid, diluted, and remaining Eu content was determined by ICP-OES.

Supplementary Material

Refer to Web version on PubMed Central for supplementary material.

Funding

E.B. acknowledges funding sources, specifically the NIH for a NIBIB R21 Trailblazer Award (Grant R21EB030071-01A1) and the National Science Foundation for an NSF CAREER (Grant CHE 1942434). K.E.M. acknowledges support through the SBU Chemistry-Biology Interface Training Program (Grants T32 GM092714 and T32 GM136572)

REFERENCES

(1). Moore EG; Samuel APS; Raymond KN From Antenna to Assay: Lessons Learned in Lanthanide Luminescence. Acc. Chem. Res 2009, 42 (4), 542–552. [PubMed: 19323456]

(2). Bünzli J-CG Lanthanide luminescence for biomedical analyses and imaging. Chem. Rev 2010, 110 (5), 2729–2755. [PubMed: 20151630]

(3). Petoud S; Cohen SM; Bünzli J-CG; Raymond KN Stable lanthanide luminescence agents highly emissive in aqueous solution: multidentate 2-hydroxyisophthalamide complexes of Sm3+, Eu3+, Tb3+, Dy3+. J.Am. Chem. Soc 2003, 125 (44), 13324–13325. [PubMed: 14583005]

(4). Xu J; Corneillie TM; Moore EG; Law G-L; Butlin NG; Raymond KN Octadentate cages of Tb (III) 2-hydroxyisophthalamides: a new standard for luminescent lanthanide labels. J. Am. Chem. Soc 2011, 133 (49), 19900–19910. [PubMed: 22010878]

(5). Xiong R; Mara D; Liu J; Van Deun R; Borbas KE Excitation- and Emission-Wavelength-Based Multiplex Spectroscopy Using Red-Absorbing Near-Infrared-Emitting Lanthanide Complexes. J. Am. Chem. Soc 2018, 140 (35), 10975–10979. [PubMed: 30122038]

(6). Hamon N; Roux A; Beyler M; Mulatier J-C; Andraud C; Nguyen C; Maynadier M; Bettache N; Duperray A; Grichine A; Brasselet S; Gary-Bobo M; Maury O; Tripier R Pyclen-Based Ln(III) Complexes as Highly Luminescent Bioprobes for In Vitro and In Vivo One- and Two-Photon Bioimaging Applications. J. Am. Chem. Soc 2020, 142 (22), 10184–10197. [PubMed: 32368907]

(7). Heffern MC; Matosziuk LM; Meade TJ Lanthanide probes for bioresponsive imaging. Chem. Rev 2014, 114 (8), 4496–4539. [PubMed: 24328202]

(8). Junker AKR; Hill LR; Thompson AL; Faulkner S; Sørensen TJ Shining light on the antenna chromophore in lanthanide based dyes. Dalton Trans. 2018, 47 (14), 4794–4803. [PubMed: 29560975]

(9). Jelley JV Cerenkov radiation and its applications. Br. J. Appl. Phys 1955, 6, 227.

(10). Thorek DL; Riedl CC; Grimm J Clinical Cerenkov luminescence imaging of 18F-FDG. J. Nucl. Med 2014, 55 (1), 95–98. [PubMed: 24078721]

(11). Roda A; Pasini P; Mirasoli M; Michelini E; Guardigli M Biotechnological applications of bioluminescence and chemiluminescence. Trends Biotechnol 2004, 22 (6), 295–303. [PubMed: 15158059]

(12). Dothager RS; Goiffon RJ; Jackson E; Harpstrite S; Piwnica-Worms D Cerenkov radiation energy transfer (CRET) imaging: A novel method for optical imaging of PET isotopes in biological systems. PLoS One 2010, 5 (10), No. e13300. [PubMed: 20949021]

(13). Ma X; Kang F; Xu F; Feng A; Zhao Y; Lu T; Yang W; Wang Z; Lin M; Wang J Enhancement of Cerenkov Luminescence Imaging by Dual Excitation of Er^{3+}, Yb^{3+}-Doped Rare-Earth Microparticles. PLoS One 2013, 8 (10), e77926. [PubMed: 24205030]

(14). Kotagiri N; Niedzwiedzki DM; Ohara K; Achilefu S Activatable probes based on distance-dependent luminescence associated with cerenkov radiation. Angew. Chem., Int. Ed 2013, 52 (30), 7756–7760.

(15). Cosby AG; Ahn SH; Boros E Cherenkov Radiation-Mediated In Situ Excitation of Discrete Luminescent Lanthanide Complexes. Angew. Chem., Int. Ed 2018, 57 (47), 15496–15499.

(16). Cosby AG; Quevedo G; Boros E A High-Throughput Method To Measure Relative Quantum Yield of Lanthanide Complexes for Bioimaging. Inorg. Chem 2019, 58, 10611–10615. [PubMed: 31380629]

(17). Li H; Tan M; Wang X; Li F; Zhang Y; Zhao L; Yang C; Chen G Temporal Multiplexed in Vivo Upconversion Imaging. J. Am. Chem. Soc 2020, 142 (4), 2023–2030. [PubMed: 31910008]

(18). Sun X; Huang X; Guo J; Zhu W; Ding Y; Niu G; Wang A; Kiesewetter DO; Wang ZL; Sun S; Chen X Self-illuminating 64Cu-doped CdSe/ZnS nanocrystals for in vivo tumor imaging. J. Am. Chem. Soc 2014, 136 (5), 1706–9. [PubMed: 24401138]

(19). Ni D; Ferreira CA; Barnhart TE; Quach V; Yu B; Jiang D; Wei W; Liu H; Engle JW; Hu P; Cai W Magnetic Targeting of Nanotheranostics Enhances Cerenkov Radiation-Induced Photodynamic Therapy. J. Am. Chem. Soc 2018, 140 (44), 14971–14979. [PubMed: 30336003]

(20). Hamon N; Roux A; Beyler M; Mulatier JC; Andraud C; Nguyen C; Maynadier M; Bettache N; Duperray A; Grichine A; Brasselet S; Gary-Bobo M; Maury O; Tripier R Pyclen-Based Ln(III) Complexes as Highly Luminescent Bioprobes for In Vitro and In Vivo One- and Two-Photon Bioimaging Applications. J. Am. Chem. Soc 2020, 142 (22), 10184–10197. [PubMed: 32368907]

(21). McMahon BK; Pal R; Parker D A bright and responsive europium probe for determination of pH change within the endoplasmic reticulum of living cells. Chem. Commun 2013, 49, 5363–5365.

(22). Walton JW; Bourdolle A; Butler SJ; Soulie M; Delbianco M; McMahon BK; Pal R; Puschmann H; Zwier JM; Lamarque L; Maury O; Andraud C; Parker D Very bright europium complexes that stain cellular mitochondria. Chem. Commun 2013, 49 (16), 1600–2.

(23). Butler SJ; Delbianco M; Lamarque L; McMahon BK; Neil ER; Pal R; Parker D; Walton JW; Zwier JM EuroTracker(R) dyes: design, synthesis, structure and photophysical properties of very bright europium complexes and their use in bioassays and cellular optical imaging. Dalton Trans. 2015, 44 (11), 4791–803. [PubMed: 25341077]

(24). Frawley AT; Linford HV; Starck M; Pal R; Parker D Enantioselective cellular localisation of europium(III) coordination complexes. Chem. Sci. 2018, 9 (4), 1042–1049. [PubMed: 29675151]

(25). Latva M; Takalo H; Mukkala VM; Matachescu C; Rodriguez-Ubis JC; Kankare J Correlation between the lowest triplet state energy level of the ligand and lanthanide(III) luminescence quantum yield. J. Lumin 1997, 75 (2), 149–169.

(26). Quici S; Gianolio E; Anelli PL; Accorsi G; Botta M; Marzanni G; Armaroli N; Cavazzini M; Barigelletti F Highly Luminescent Eu 3+ and Tb 3+ Macrocyclic Complexes Bearing an Appended Phenanthroline Chromophore. Inorg. Chem 2002, 41 (10), 2777–2784. [PubMed: 12005503]

(27). Beeby A; Parker D; de Sousa AS; Clarkson IM; Woods M; Faulkner S; Dickins RS; Royle L; Williams JAG Non-radiative deactivation of the excited states of europium, terbium and ytterbium complexes by proximate energy-matched OH, NH and CH oscillators: an improved luminescence method for establishing solution hydration states. J. Chem. Soc., Perkin Trans. 2 1999, 2 (3), 493–504.

(28). Newkome GR; Theriot KJ; Gupta VK; Fronczek FR; Baker GR Chemistry of heterocyclic compounds. 124. Mono-α-functionalization of 2,9-dimethyl-l,10-Phenanthroline. J. Org. Chem 1989, 54 (7), 1766–1769.

(29). Kikuchi K; Sugihara F; Mizukami S; Yoshioka Y; Matsushita H; Nakamura T Activatable 19 F MRI Nanoparticle Probes for the Detection of Reducing Environments. Angew. Chem., Int. Ed 2015, 54 (3), 1007–1010.

(30). Lim N-H; Ding-Pfennigdorff D; Nagase H; Hu H-Y; Wendt KU; Schultz C; Plettenburg O; Saas J; Nazare M; Ritzeler O DOTAM Derivatives as Active Cartilage-Targeting Drug Carriers for the Treatment of Osteoarthritis. Bioconjugate Chem. 2015, 26 (3), 383–388.

(31). Brouwer AM Standards for photoluminescence quantum yield measurements in solution (IUPAC Technical Report). Pure Appl. Chem 2011, 83 (12), 2213–2228.

(32). Van Houten J; Watts RJ The Effect of Ligand and Solvent Deuteration on the Excited State Properties of the Tris(2,2'-bipyridyl)ruthenium(II) Ion in Aqueous Solution. Evidence for Electron Transfer to Solvent. J. Am. Chem. Soc 1975, 97 (13), 3843–3844.

(33). Thiele NA; Woods JJ; Wilson JJ Implementing f-Block Metal Ions in Medicine: Tuning the Size Selectivity of Expanded Macrocycles. Inorg. Chem 2019, 58 (16), 10483–10500. [PubMed: 31246017]

(34). Aluicio-Sarduy E; Thiele NA; Martin KE; Vaughn BA; Devaraj J; Olson AP; Barnhart TE; Wilson JJ; Boros E; Engle JW Establishing Radiolanthanum Chemistry for Targeted Nuclear Medicine Applications. Chem. - Eur. J 2020, 26 (6), 1238–1242. [PubMed: 31743504]

(35). Thiele NA; Brown V; Kelly JM; Amor-Coarasa A; Jermilova U; MacMillan SN; Nikolopoulou A; Ponnala S; Ramogida CF; Robertson AKH; Rodríguez-Rodríguez C; Schaffer P; Williams C Jr.; Babich JW; Radchenko V; Wilson JJ An Eighteen-Membered Macrocyclic Ligand for Actinium-225 Targeted Alpha Therapy. Angew. Chem., Int. Ed 2017, 56 (46), 14712–14717.

(36). Meimetis LG; Boros E; Carlson JC; Ran C; Caravan P; Weissleder R Bioorthogonal Fluorophore Linked DFO - Technology Enabling Facile Chelator Quantification and Multimodal Imaging of Antibodies. Bioconjugate Chem. 2016, 27 (1), 257–263.

(37). Adams CJ; Wilson JJ; Boros E Multifunctional Desferrichrome Analogues as Versatile 89Zr(IV) Chelators for ImmunoPET Probe Development. Mol. Pharmaceutics 2017, 14 (8), 2831–2842.

(38). Xu J; Zhou J; Chen Y; Yang P; Lin J Lanthanide-activated nanoconstructs for optical multiplexing. Coord. Chem. Rev 2020, 415, 213328.

(39). Kularatne SA; Zhou Z; Yang J; Post CB; Low PS Design, Synthesis, and Preclinical Evaluation of Prostate-Specific Membrane Antigen Targeted 99m Tc-Radioimaging Agents. Mol. Pharmaceutics 2009, 6 (3), 790–800.

(40). Ghosh A; Heston WDW Tumor target prostate specific membrane antigen (PSMA) and its regulation in prostate cancer. J. Cell. Biochem 2004, 91 (3), 528–539. [PubMed: 14755683]

(41). Chen Y; Pullambhatla M; Banerjee SR; Byun Y; Stathis M; Rojas C; Slusher BS; Mease RC; Pomper MG Synthesis and Biological Evaluation of Low Molecular Weight Fluorescent Imaging Agents for the Prostate-Specific Membrane Antigen. Bioconjugate Chem. 2012, 23, 2377–2385.

(42). Baranski AC; Schäfer M; Bauder-Wüst U; Roscher M; Schmidt J; Stenau E; Simpfendörfer T; Teber D; Maier-Hein L; Hadaschik B; Haberkorn U; Eder M; Kopka K PSMA-11-Derived dual-Labeled PSMA inhibitors for preoperative PET imaging and precise fluorescence-Guided surgery of prostate cancer. J. Nucl Med 2018, 59 (4), 639–645. [PubMed: 29191856]

(43). Hensbergen AW; Van Willigen DM; Van Beurden F; Van Leeuwen PJ; Buckle T; Schottelius M; Maurer T; Wester HJ; Van Leeuwen FWB Image-Guided Surgery: Are We Getting the Most out of Small-Molecule Prostate-Specific-Membrane-Antigen-Targeted Tracers? Bioconjugate Chem. 2020, 31 (2), 375–395.

(44). Gale EM; Jones CM; Ramsay I; Farrar CT; Caravan P A Janus Chelator Enables Biochemically Responsive MRI Contrast with Exceptional Dynamic Range. J. Am. Chem. Soc 2016, 138 (49), 15861–15864. [PubMed: 27960350]

(45). Wang H; Jordan VC; Ramsay IA; Sojoodi M; Fuchs BC; Tanabe KK; Caravan P; Gale EM Molecular Magnetic Resonance Imaging Using a Redox-Active Iron Complex. J. Am. Chem. Soc 2019, 141 (14), 5916–5925. [PubMed: 30874437]

(46). Yu M; Bouley BS; Xie D; Enriquez JS; Que EL (19)F PARASHIFT Probes for Magnetic Resonance Detection of H2O2 and Peroxidase Activity. J. Am. Chem. Soc 2018, 140 (33), 10546–10552. [PubMed: 30052043]

(47). Abdelfattah AS; Kawashima T; Singh A; Novak O; Liu H; Shuai Y; Huang Y-C; Campagnola L; Seeman SC; Yu J; Zheng J; Grimm JB; Patel R; Friedrich J; Mensh BD; Paninski L; Macklin JJ; Murphy GJ; Podgorski K; Lin B-J; Chen T-W; Turner GC; Liu Z; Koyama M; Svoboda K; Ahrens MB; Lavis LD; Schreiter ER Bright and photostable chemigenetic indicators for extended in vivo voltage imaging. Science 2019, 365 (6454), 699–704. [PubMed: 31371562]

(48). He S; Li J; Lyu Y; Huang J; Pu K Near-Infrared Fluorescent Macromolecular Reporters for Real-Time Imaging and Urinalysis of Cancer Immunotherapy. J. Am. Chem. Soc 2020, 142 (15), 7075–7082. [PubMed: 32196318]

(49). Ning Y; Liu YW; Yang ZS; Yao Y; Kang L; Sessler JL; Zhang JL Split and Use: Structural Isomers for Diagnosis and Therapy. J. Am. Chem. Soc 2020, 142 (14), 6761–6768. [PubMed: 32172565]

(50). Yang Y; Zhou T; Jin M; Zhou K; Liu D; Li X; Huo F; Li W; Yin C Thiol-Chromene “Click” Reaction Triggered Self-Immolative for NIR Visualization of Thiol Flux in Physiology and Pathology of Living Cells and Mice. J. Am. Chem. Soc 2020, 142 (3), 1614–1620. [PubMed: 31887253]

(51). Ye D; Shuhendler AJ; Cui L; Tong L; Tee SS; Tikhomirov G; Felsher DW; Rao J Bioorthogonal cyclization-mediated in situ self-assembly of small-molecule probes for imaging caspase activity in vivo. Nat. Chem 2014, 6 (6), 519–26. [PubMed: 24848238]

(52). Chen Z; Mu X; Han Z; Yang S; Zhang C; Guo Z; Bai Y; He W An Optical/Photoacoustic Dual-Modality Probe: Ratiometric in/ex Vivo Imaging for Stimulated H2S Upregulation in Mice. J. Am. Chem. Soc 2019, 141 (45), 17973–17977. [PubMed: 31657918]

(53). Boss M; Bos D; Frielink C; Sandker G; Ekim S; Marciniak C; Pattou F; van Dam G; van Lith S; Brom M; Gotthardt M; Buitinga M Targeted Optical Imaging of the Glucagonlike Peptide 1 Receptor Using Exendin-4-IRDye 800CW. J. Nucl. Med 2020, 61 (7), 1066–1071. [PubMed: 31924726]

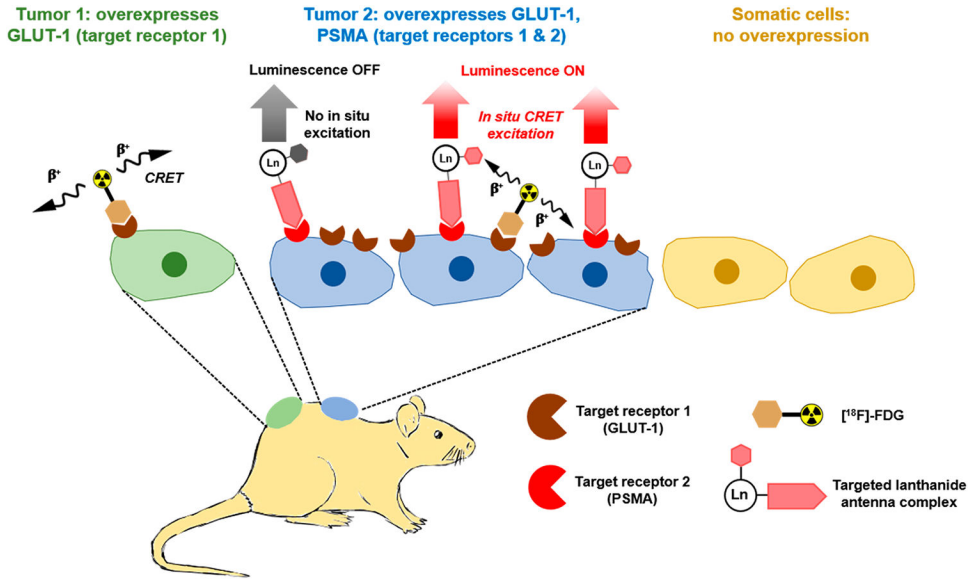

Figure 1.

Schematic depiction of the in situ CRET-mediated excitation of discrete, targeted Ln(III) complexes. Specifically, we propose to use the clinically employed PET agent [^{18}F]-FDG as a CRET source that exhibits uptake in cancer cells broadly due to the overexpression of GLUT-1 transporters. Here, we propose that discrete luminescent lanthanide complexes functionalized with a targeting vector that is only expressed in a subpopulation of cancer cells can be used to selectively illuminate these cells when colocalized with the CR source. The in situ excitation of these probes enables wavelength selective multiplex imaging and the detection of long wave emission of Ln(III) complexes with conventional optical imaging tools, obviating the need for high intensity laser excitation sources or time-resolved luminescence detection.

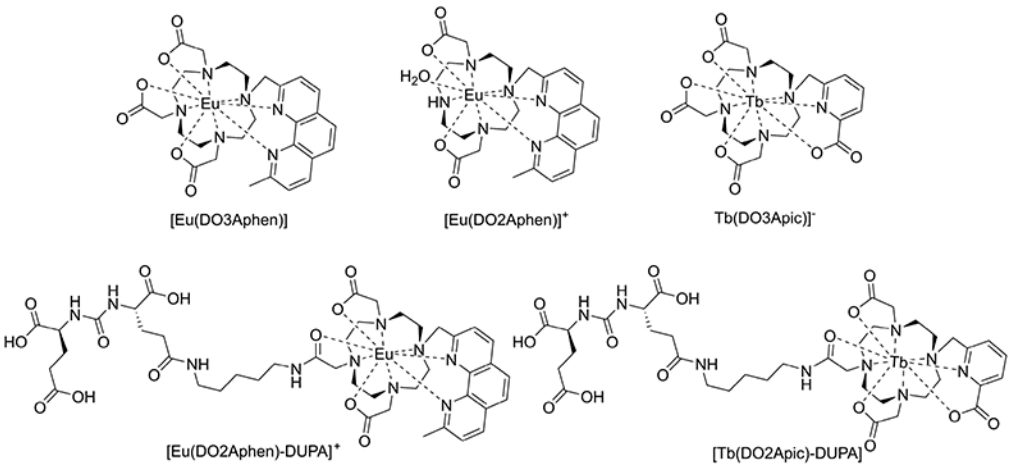

Figure 2.
Complexes explored in this work.

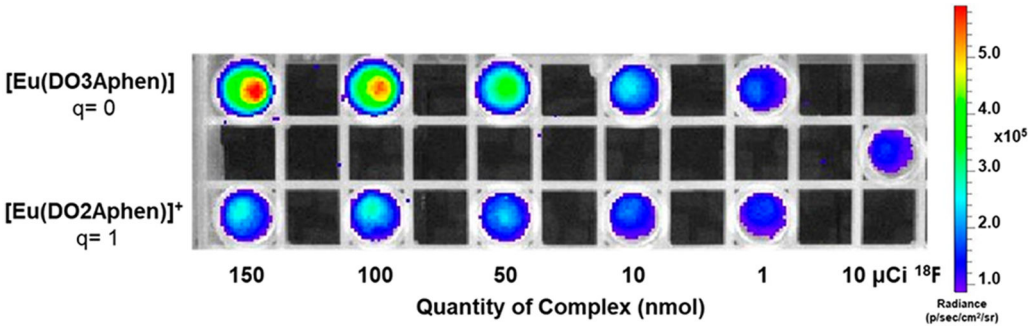

Figure 3.

CRET excitation of [Eu(DO3Aphen)] and $[Eu(DO2Aphen)]^{+}$ showing the impact of hydration on radiance output.

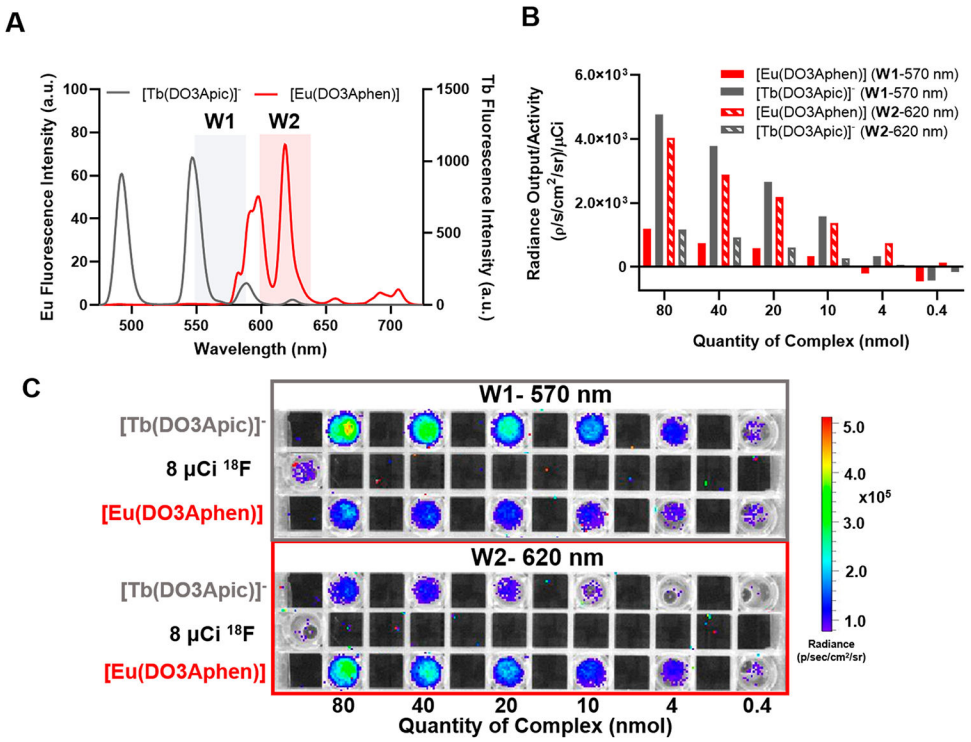

Figure 4.

Multiplexed imaging of nonfunctionalized complexes: (A) emission filter windows (W1, 570 nm; W2, 620 nm) overlaid with the luminescence spectra of [Eu(DO3Aphen)] and $[Tb(DO3Apic)]^{-}$; (B) quantified radiance of the complexes in the presence of 8 μCi of $Na^{18}F$ using region of interest analysis; (C) phantom images of the nonfunctionalized complexes with emission filters (W1 and W2) in the presence of 8 μCi of $Na^{18}F$.

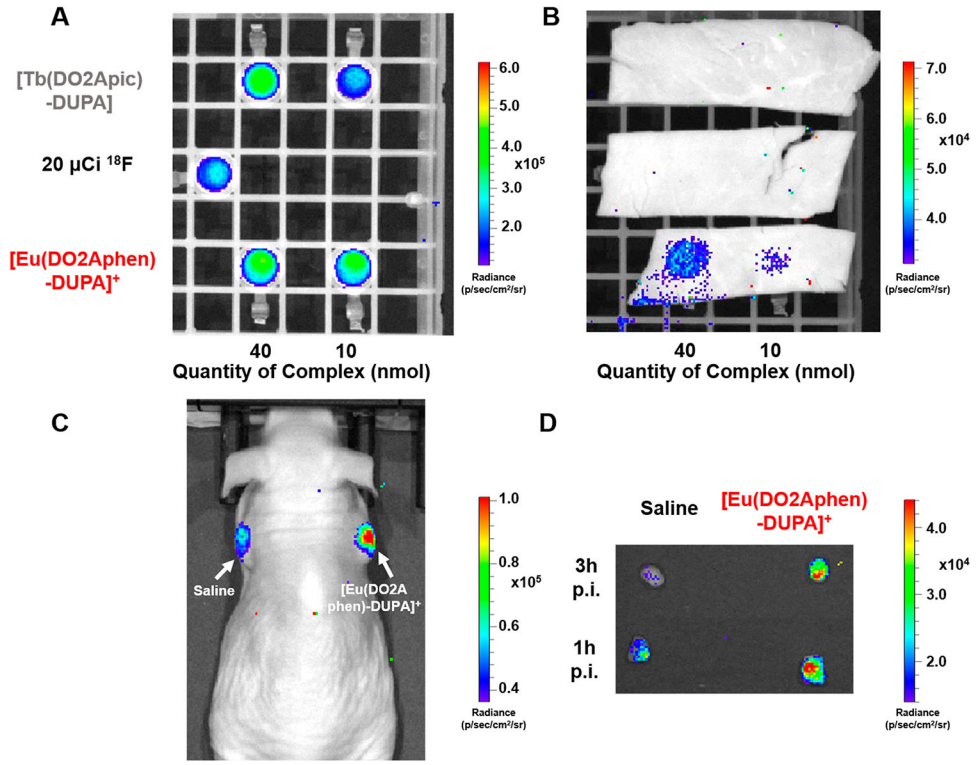

Figure 5.

(A) Phantom image of 40 and 10 nmol of [Tb(DO2Apic)-DUPA] and [Eu(DO2Aphen)-DUPA]$^{+}$ in the presence of 20 μCi Na^{18}F. (B) Samples shown in (A) overlaid with 2 mm tissue sample (muscle) demonstrating detectable emission for 40 and 10 nmol of [Eu(DO2Aphen)-DUPA]$^{+}$. (C) In vivo optical imaging of 22 μCi [^{18}F]-FDG and 40 nmol [Eu(DO2Aphen)-DUPA]$^{+}$ probe at 8 min following intratumoral administration. (D) Excised tumors imaged at 1 and 3 h postinjection (p.i.) demonstrate the persistent, detectable emission signal of [Eu(DO2Aphen)-DUPA]$^{+}$. Tissue digestion and subsequent quantitation of residual Eu(III) indicate retention of 53% ID/g of the administered probe.

Table 1.

Photophysical Characterization Including Gradient-Based QY (Φ_{Ln}), Inner-Sphere Hydration Number (q), and Luminescent Lifetimes (τ) Determined in H_2O or D_2O

complex	Φ_{Ln} [a] (%)	τ, H_2O (ms)	τ, D_2O (ms)	q [b]
[Eu(DO3Aphen)]	15	1.27	1.79	0
$[Eu(DO2Aphen)]^+$	5	0.58	1.82	1.11
$[Eu(DO2Aphen)\text{-}DUPA]^+$	10	1.17	1.73	0
$[Tb(DO3Apic)]^-$ [15]	47	2.83	2.75	0
[Tb(DO2Apic)-DUPA]	38	1.09	1.13	0

[a] Reported with an error of ±10–15%.

[b] Reported with an error of ±20%.[27]